Hindawi
Mathematical Problems in Engineering
Volume 2017, Article ID 6062798, 14 pages
https://doi.org/10.1155/2017/6062798

Research Article

Stability Analysis Method of Parallel Inverter

Jun Li,[1] Jie Chen,[1] Yaru Xue,[1] Ruichang Qiu,[2] and Zhigang Liu[1]

[1]*School of Electrical Engineering, Beijing Jiaotong University, Beijing, China*
[2]*Beijing Rail Transit Electrical Engineering Technology Research Center, Beijing, China*

Correspondence should be addressed to Jie Chen; jiechen@bjtu.edu.cn

Received 12 May 2017; Accepted 13 August 2017; Published 2 November 2017

Academic Editor: Zoran Gajic

In order to further provide theoretical support for the stability of an auxiliary inverter parallel system, a new model which covers most of control parameters needs to be established. However, the ability of the small-signal model established by the traditional method is extremely limited, so this paper proposes a new small-signal modeling method for the parallel system. The new small-signal model not only can analyze the influence of the droop parameters on the system performance, but also can analyze the influence of the output impedance of the inverter, the unbalanced and nonlinear loads, and the power calculation method and cut-off frequency of the low-pass filter on the system performance and stability. Based on this method, this paper carries out a comprehensive analysis on the performance of a parallel inverter system. And the correctness of the modeling method and analysis process of the system performance and stability are verified by the consistency of the simulation and experimental results.

1. Introduction

The stability of a parallel system is one of the important indexes to evaluate the performance of a parallel system. For a high power auxiliary parallel system, a change of the various control parameters has an extremely large impact on the stability of the system. Therefore, it is very important and necessary to analyze the stability of the parallel system.

In general, the stability analysis of a parallel system should be based on a specific parallel control strategy. At present, the wireless parallel system usually adopts the droop method to achieve current sharing automatically [1–6], the basic approach of which is to use active power and reactive power to droop the amplitude and frequency of the voltage. The paper also adopts the droop method but has been modified to improve effectively [7–10] and the whole cycle adaptive droop method (TWCADM) is proposed. It is pointed out that a new power calculation method without a large delay low-pass filter, combined with the improved droop method, can greatly enhance the dynamic response of the parallel system. However, the author does not demonstrate the reason of the improvement of dynamic response in theory. Therefore, it is necessary to establish a unified model of the parallel system, using the mathematical tools to prove the improvement of the dynamic response in theory.

For the mathematical model of a parallel inverter system, the relevant literature [11, 12] is not abundant. Antonio et al. establish a small-signal model of grid-connected inverter for the first time [13], but he only considers the outer power loop and regards the inner voltage loop as the ideal state. This method is relatively simple, the established model is of 3rd-order, and, to a certain extent, it can reflect the change trend of a single inverter. However, a big drawback of this method is that the voltage of the parallel point is regarded as an independent variable, so that the parallel inverter automatically shields the influence of another inverter, and most papers adopt this method [14–16]. Marwali et al. propose a small-signal modeling method which can consider the whole parallel system [17], and the voltage of a parallel point can be expressed as the physical variable of each inverter. All inverters in a parallel system can be coupled together by the voltage at a parallel point, and the inverters in the model can affect each other, so the established model is more accurate. But in Marwali et al.'s paper, the model established by the discrete modeling method in the Z domain

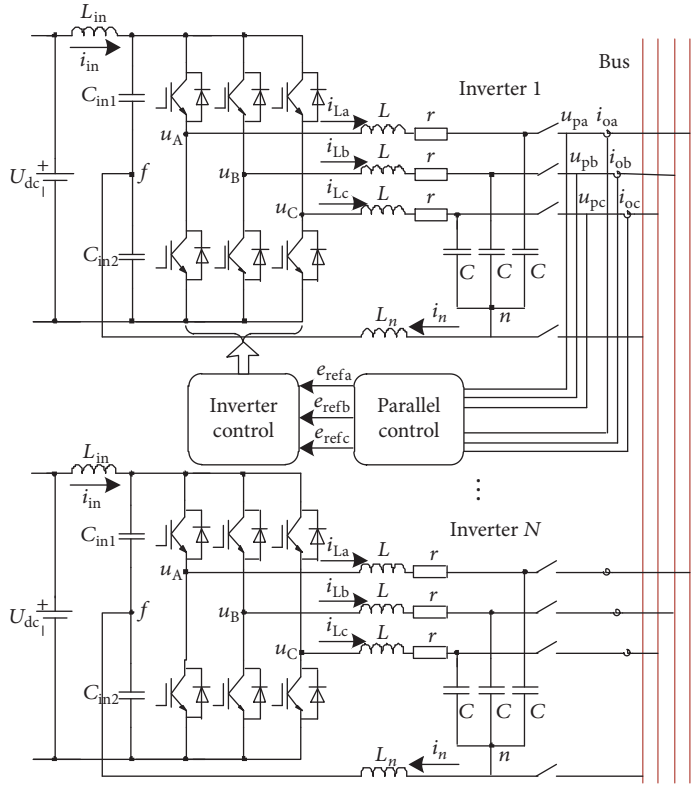

Figure 1: The topology of auxiliary parallel inverter system.

is extremely complex. Actually, it is not greatly significant for the parallel system with large delay link to adopt discrete analysis; besides, this method fails to take the impact of the power calculation method into account.

Aiming at the defects of the methods above, this paper proposes a new method to establish the small-signal model of a parallel system, which can take the factors into account such as the coupling effect between the inverters in the parallel system, the influence of the line parameters, load characteristics, and the power calculation method and the cut-off frequency of the low-pass filter. The model established by this method can effectively analyze the influence of each correlation variable of the parallel inverter on the system performance, has a very wide universality, and is simpler than the model established by Marwali et al.

2. The Control Method of Parallel Inverters

Figure 1 is the topology of the parallel system, which indicates that the inverter adopts the three-phase four-wire system with split capacitor topology, and each inverter is controlled in two stages: parallel control [18–23] and inverter control [24–28], and the output voltage and output current of each phase need to be sampled.

Figure 2 is the schematic diagram of inverter control and we can obtain the output voltage of the inverter from the diagram:

$$u_o = G(s)\, u_{ref} - Z(s)\, i_o, \tag{1}$$

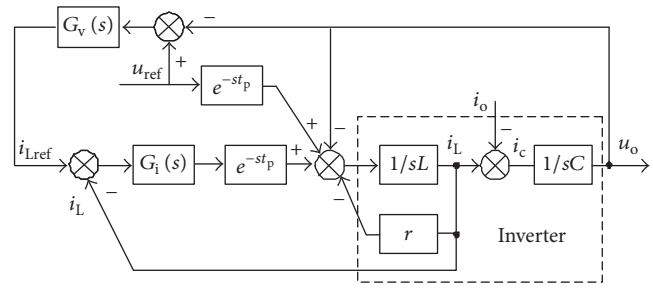

Figure 2: The schematic diagram of inverter control.

where

$$G(s) = \frac{\left[G_v(s)\, G_i(s) + 1\right] e^{-st_p}}{G_v(s)\, G_i(s)\, e^{-st_p} + sCG_v(s)\, e^{-st_p} + LCs^2 + rCs + 1},$$
$$Z(s) = \frac{G_i(s)\, e^{-st_p} + sL + r}{G_v(s)\, G_i(s)\, e^{-st_p} + sCG_i(s)\, e^{-st_p} + LCs^2 + rCs + 1}. \tag{2}$$

In (1), $G(s)$ is control branch and $Z(s)$ is inverter internal impedance. Equation (1) indicates that both $G(s)$ and $Z(s)$ can be controlled by the voltage controller $G_v(s)$ and the current controller $G_i(s)$. If the appropriate voltage controller

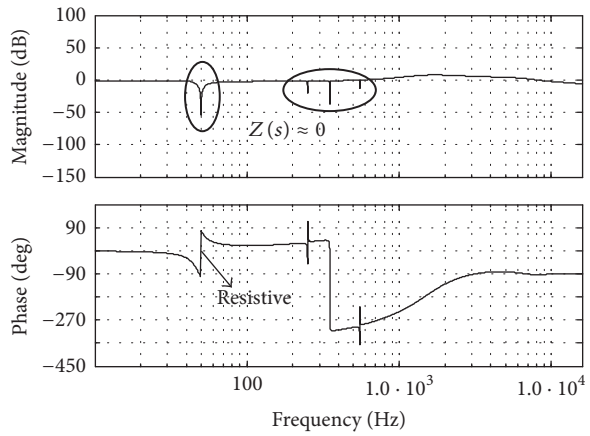

Figure 3: The bode diagram of the internal impedance of the inverter.

and current controller are selected, the internal impedance of the inverter can be designed.

In this paper, the improved resonant controller is used as the voltage controller and a proportional controller is used as the current controller.

Figure 3 is the bode diagram of the internal impedance of the inverter and we can discover an interesting result that the method shown in Figure 2 leads the internal impedance to be resistive. Therefore, the resistive droop method is suitable for the parallel system:

$$\begin{aligned} E_{\text{ref}} &= E_0 - \left(m_{\text{p}} + m_{\text{d}}s\right)P, \\ \varphi_{\text{ref}} &= \varphi_0 - \left(n_{\text{p}} + \frac{n_{\text{i}}}{s} + n_{\text{d}}s\right)Q, \end{aligned} \tag{3}$$

where m_{p} is the proportion a droop coefficient of active power, m_{d} is the differential coefficient of active power, n_{p} is the proportion of a droop coefficient of reactive power, n_{i} is the integral coefficient of reactive power, and n_{d} is the differential coefficient of reactive power. P and Q represent the active power and reactive power, respectively, and both of them are the values after the large delay low-pass filter.

Traditionally, the power calculation method is described by the following equation:

$$\begin{aligned} \widetilde{p} &= \dot{U}\dot{I}_{\text{o}}, \\ \widetilde{q} &= -\dot{U}\left(\dot{I}_{\text{o}}\angle -90^{\circ}\right), \end{aligned} \tag{4}$$

where

$$\begin{aligned} \dot{U} &= U_{\max}\cos\left(\omega t + \theta_{\text{u}}\right), \\ \dot{I}_{\text{o}} &= I_{\max}\cos\left(\omega t + \theta_{\text{i}}\right). \end{aligned} \tag{5}$$

In (5), $U_{\max}$ is the maximum value of voltage, θ_{u} is the initial voltage phase angle, $I_{\max}$ is the maximum value of current, and θ_{i} is the initial current phase angle.

In the power calculation method above, the obtained power contains an AC component at two-times the fundamental frequency. Therefore, a large delay low-pass filter is adopted to filter the AC component, which deteriorates the dynamic performance of the parallel system.

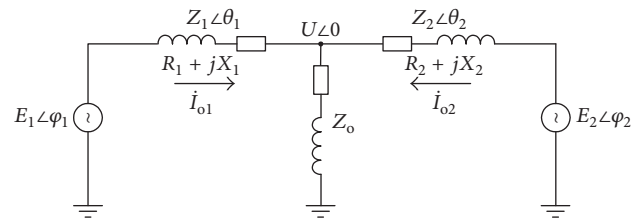

Figure 4: The model of a parallel inverter.

In order to improve the dynamic performance of the parallel system, the power calculation method can be improved as the following equation:

$$\begin{aligned} \widetilde{p} &= 0.5\dot{U}\dot{I}_{\text{o}} + 0.5\left(\dot{U}\angle -90^{\circ}\right)\left(\dot{I}_{\text{o}}\angle -90^{\circ}\right), \\ \widetilde{q} &= 0.5\left(\dot{U}\angle -90^{\circ}\right)\dot{I}_{\text{o}} - 0.5\dot{U}\left(\dot{I}_{\text{o}}\angle -90^{\circ}\right). \end{aligned} \tag{6}$$

Equation (6) indicates that both the voltage and current need to be delayed by 90 degrees which leads to more storage cost payment. However, the obtained power does not contain an AC component any more, which enables the cut-off frequency to be set higher, and the dynamic performance of parallel system can be effectively enhanced, as shown in

$$\begin{aligned} P &= \widetilde{p}\frac{\omega_{\text{c}}}{s+\omega_{\text{c}}}, \\ Q &= \widetilde{q}\frac{\omega_{\text{c}}}{s+\omega_{\text{c}}}. \end{aligned} \tag{7}$$

3. The Traditional Small-Signal Modeling Method

According to the above derivation, we can simplify the parallel inverter model, as shown in Figure 4, where $Z\angle\theta$ is the output impedance of the inverter, consisting of two parts: internal impedance and line impedance.

From Figure 4, according to the concept of complex power, the output power of the inverter can be obtained:

$$\begin{aligned} P &= \frac{1}{R^2+X^2}\left(UER\cos\varphi + UEX\sin\varphi - U^2R\right), \\ Q &= \frac{1}{R^2+X^2}\left(-UER\sin\varphi + UEX\cos\varphi - U^2X\right). \end{aligned} \tag{8}$$

Considering the small disturbance existing near the steady-state value $(E, E_{\text{e}}, U_{\text{e}})$, (8) can be linearised as

$$\Delta P = \Delta E\alpha - \Delta\varphi E\beta, \tag{9}$$

$$\Delta Q = -\Delta E\beta - \Delta\varphi E\alpha, \tag{10}$$

where

$$\begin{aligned} \alpha &= \frac{1}{R^2+X^2}\left(UR\cos\varphi + UX\sin\varphi\right), \\ \beta &= \frac{1}{R^2+X^2}\left(UR\sin\varphi - UX\cos\varphi\right). \end{aligned} \tag{11}$$

Based on the droop method mentioned in (3), the differential calculation result can be obtained as follows:

$$\Delta E = -\left(m_p + m_d s\right)\Delta P, \tag{12}$$

$$\Delta\varphi = \left(n_p + \frac{n_i}{s} + n_d s\right)\Delta Q. \tag{13}$$

Combining (9), (10), (12), (13), and (7), $\Delta\varphi$ and ΔE can be obtained:

$$\begin{aligned}\Delta\varphi &= \frac{\omega_c}{s+\omega_c}\left(n_p + n_i\frac{1}{s} + n_d s\right)\left(-\Delta E\beta - \Delta\varphi E\alpha\right),\\ \Delta E &= \frac{\omega_c}{s+\omega_c}\left(-m_p - m_d s\right)\left(\Delta E\alpha - \Delta\varphi E\beta\right).\end{aligned} \tag{14}$$

Simplifying (14) the small-signal model can be obtained as follows:

$$s^3\Delta\varphi + As^2\Delta\varphi + Bs\Delta\varphi + C\Delta\varphi = 0, \tag{15}$$

where

$$\begin{aligned}A &= \frac{\left(\alpha m_p + \alpha\omega_c m_d\right) + E\omega_c\left(\alpha^2+\beta^2\right)\left(n_d m_p + n_p m_d\right)}{\alpha m_d + E\omega_c\left(\alpha^2+\beta^2\right)n_d m_d},\\ B &= \frac{\alpha\omega_c m_p + E\omega_c\left(\alpha^2+\beta^2\right)\left(n_i m_d + n_p m_p\right)}{\alpha m_d + E\omega_c\left(\alpha^2+\beta^2\right)n_d m_d},\\ C &= \frac{E\omega_c\left(\alpha^2+\beta^2\right)n_i m_p}{\alpha m_d + E\omega_c\left(\alpha^2+\beta^2\right)n_d m_d}.\end{aligned} \tag{16}$$

Equation (15) is the traditional small-signal model, and it can be found that the traditional model is of 3rd-order, so the traditional small-signal modeling method is relatively simple and apt to analyze. However, this method is not accurate, mainly for the following reasons:

(1) The voltage at the parallel point is regarded as an independent variable, and the coupling effect between two inverters is eliminated. However, for an actual parallel system, there must be a coupling action between the two inverters, and the change of output characteristics of one inverter will inevitably lead to that of the other inverter. Therefore, the traditional small-signal modeling method is not accurate.

(2) It is well known that the load characteristics have a great impact on the stability of the parallel system, but the traditional small-signal model cannot analyze the influence of the load characteristics.

(3) The traditional small-signal model cannot analyze the influence of different power calculation methods.

4. The New Small-Signal Modeling Method

Aiming at the drawbacks of the traditional small-signal modeling method, this paper proposes a new small-signal modeling method. The model established by this modeling method has a wide enough amount of information and it can not only analyze most of the control parameters outside the voltage loop of the control system but also analyze the influence of the circuit parameters. What is more, the model is simpler than the model established by Marwali et al. [17].

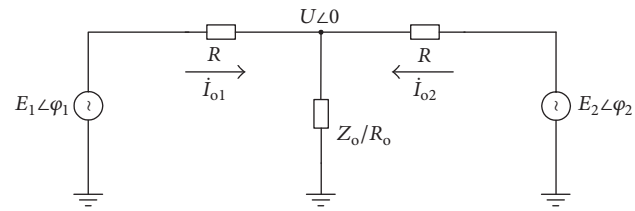

Figure 5: Simplified parallel model.

For convenience, the parallel system shown in Figure 4 can be simplified as shown in Figure 5. The simplification is just to simplify the modeling and description process; readers can restore the output impedance of inverter and the load into any characteristics; it is even possible to consider the influence of two inverters on the parallel system with inconsistent impedance characteristics.

Based on Figure 5, the output current of the inverter can be obtained as

$$\begin{aligned}\dot{I}_{o1} &= \frac{\left(\dot{E}_1 - \dot{U}\right)}{R},\\ \dot{I}_{o2} &= \frac{\left(\dot{E}_2 - \dot{U}\right)}{R}.\end{aligned} \tag{17}$$

The sum of the output current of two inverters is the load current and the output voltage can be obtained by the load current as

$$\dot{U} = R_o\dot{I}_{o1} + R_o\dot{I}_{o2}. \tag{18}$$

Combining (17) and (18), we can obtain

$$\dot{U} = \frac{R_o\left[E_1\cos\varphi_1 + E_2\cos\varphi_2 + j\left(E_1\sin\varphi_1 + E_2\sin\varphi_2\right)\right]}{R + 2R_o}. \tag{19}$$

From Figure 5, we can discover that the voltage phase angle at the parallel point is zero. In fact, the parallel voltage is sinusoidal and the phase angel is varied, and, for the convenience of modeling, the phase angel is set to the reference value so the phase angle φ_1 and φ_2 can be understood as the phase angle difference, rather than a time varying variable. The meaning of the equivalence is that the time varying variable can be transformed into an invariant, which is suitable for analysis at the small-signal model.

According to (19), we can get two equations as follows.

$$U = \frac{R_o\left(E_1\cos\varphi_1 + E_2\cos\varphi_2\right)}{R + 2R_o}, \tag{20}$$

$$0 = E_1\sin\varphi_1 + E_2\sin\varphi_2. \tag{21}$$

Equation (20) specifies the relationship between the parameters of the two inverters and the parallel point voltage.

Equation (21) specifies the relationship between the steady-state voltages of the inverters.

Combining (19) and (17), we can obtain

$$\begin{aligned}\dot{I}_{o1} &= \frac{E_1\cos\varphi_1\left(R+R_o\right)-R_oE_2\cos\varphi_2}{R\left(R+2R_o\right)} \\ &\quad+\frac{j\left[E_1\sin\varphi_1\left(R+R_o\right)-R_oE_2\sin\varphi_2\right]}{R\left(R+2R_o\right)}, \\ \dot{I}_{o2} &= \frac{E_2\cos\varphi_2\left(R+R_o\right)-R_oE_1\cos\varphi_1}{R\left(R+2R_o\right)} \\ &\quad+\frac{j\left[E_2\sin\varphi_2\left(R+R_o\right)-R_oE_1\sin\varphi_1\right]}{R\left(R+2R_o\right)}.\end{aligned} \tag{22}$$

According to the traditional power calculation method [29, 30], we can find that before the power calculation we need to obtain $\dot{I}_o\angle -90^\circ$. In practical operation, the current waveform can be stored in electronic memory in real time. However, in the process of stability analysis, it is known that $\dot{I}_o\angle -90^\circ$ is actually the result of the exchange between the real part and imaginary part of $\dot{I}_o$, so we can obtain

$$\begin{aligned}\dot{I}_{o1}\angle -90^\circ &= \frac{E_1\sin\varphi_1\left(R+R_o\right)-R_oE_2\sin\varphi_2}{R\left(R+2R_o\right)} \\ &\quad-\frac{j\left[E_1\cos\varphi_1\left(R+R_o\right)-R_oE_2\cos\varphi_2\right]}{R\left(R+2R_o\right)},\end{aligned} \tag{23}$$

$$\begin{aligned}\dot{I}_{o2}\angle -90^\circ &= \frac{E_2\sin\varphi_2\left(R+R_o\right)-R_oE_1\sin\varphi_1}{R\left(R+2R_o\right)} \\ &\quad-\frac{j\left[E_2\cos\varphi_2\left(R+R_o\right)-R_oE_1\cos\varphi_1\right]}{R\left(R+2R_o\right)}.\end{aligned} \tag{24}$$

Combining (20), (23), and (24), we can get the traditional power calculation method:

$$\begin{aligned}p_i &= a_i + jb_i, \\ q_i &= c_i + jd_i,\end{aligned} \tag{25}$$

where, a_i, b_i, c_i, and d_i can be expressed by the inverter parameters which are given in Appendix C. Similarly, adopting the same method, a new method of power calculation can be obtained, which is the same as (25). And only the values of a_i, b_i, c_i, and d_i are different, and they are given in Appendix D.

Using the droop method mentioned in (3):

$$\begin{aligned}E_i &= E_{i0}-\frac{\left(m_p+m_ds\right)\omega_c}{s+\omega_c}p_i, \\ \varphi_i &= \varphi_{i0}+\frac{\left(n_ds^2+n_ps+n_i\right)\omega_c}{s\left(s+\omega_c\right)}q_i.\end{aligned} \tag{26}$$

Differentiating (26) near the steady-state value $(E_{1e}, E_{2e}, \varphi_{1e}, \varphi_{2e})$, we can obtain (27).

$$\begin{bmatrix}\Delta E_1\\ \Delta\varphi_1\\ \Delta E_2\\ \Delta\varphi_2\end{bmatrix}=\begin{bmatrix}-\dfrac{\omega_c\left(m_p+m_ds\right)}{s+\omega_c}\Delta p_1\\ \dfrac{\omega_c\left(n_ds^2+n_ps+n_i\right)}{s\left(s+\omega_c\right)}\Delta q_1\\ -\dfrac{\omega_c\left(m_p+m_ds\right)}{s+\omega_c}\Delta p_2\\ \dfrac{\omega_c\left(n_ds^2+n_ps+n_i\right)}{s\left(s+\omega_c\right)}\Delta q_2\end{bmatrix}, \tag{27}$$

$$\begin{bmatrix}\Delta p_1\\ \Delta q_1\\ \Delta p_2\\ \Delta q_2\end{bmatrix}=D\begin{bmatrix}\Delta\varphi_1\\ \Delta\varphi_2\\ \Delta E_1\\ \Delta E_2\end{bmatrix}, \tag{28}$$

where D is the coefficient matrix:

$$D=\begin{bmatrix}d_{11} & d_{12} & d_{13} & d_{14}\\ d_{21} & d_{22} & d_{23} & d_{24}\\ d_{31} & d_{32} & d_{33} & d_{34}\\ d_{41} & d_{42} & d_{43} & d_{44}\end{bmatrix}. \tag{29}$$

Combining (28) and (29), we can obtain the small-signal model of the parallel system, as shown in (30). The coefficients in the equation are given in Appendix.

Similarly, we can construct the small-signal model based on the new power calculation method; the model is still as shown in (30), but the coefficients are slightly different; please refer to Appendix.

$$\begin{vmatrix}-d_{11}\dfrac{\omega_c\left(m_p+m_ds\right)}{s+\omega_c} & -d_{12}\dfrac{\omega_c\left(m_p+m_ds\right)}{s+\omega_c} & -d_{13}\dfrac{\omega_c\left(m_p+m_ds\right)}{s+\omega_c}-1 & -d_{14}\dfrac{\omega_c\left(m_p+m_ds\right)}{s+\omega_c}\\ d_{21}\dfrac{s\left(s+\omega_c\right)}{\omega_c\left(n_ds^2+n_ps+n_i\right)}-1 & d_{22}\dfrac{s\left(s+\omega_c\right)}{\omega_c\left(n_ds^2+n_ps+n_i\right)} & d_{23}\dfrac{s\left(s+\omega_c\right)}{\omega_c\left(n_ds^2+n_ps+n_i\right)} & d_{24}\dfrac{s\left(s+\omega_c\right)}{\omega_c\left(n_ds^2+n_ps+n_i\right)}\\ -d_{31}\dfrac{\omega_c\left(m_p+m_ds\right)}{s+\omega_c} & -d_{32}\dfrac{\omega_c\left(m_p+m_ds\right)}{s+\omega_c} & -d_{33}\dfrac{\omega_c\left(m_p+m_ds\right)}{s+\omega_c} & -d_{34}\dfrac{\omega_c\left(m_p+m_ds\right)}{s+\omega_c}-1\\ d_{41}\dfrac{s\left(s+\omega_c\right)}{\omega_c\left(n_ds^2+n_ps+n_i\right)} & d_{42}\dfrac{s\left(s+\omega_c\right)}{\omega_c\left(n_ds^2+n_ps+n_i\right)}-1 & d_{43}\dfrac{s\left(s+\omega_c\right)}{\omega_c\left(n_ds^2+n_ps+n_i\right)} & d_{44}\dfrac{s\left(s+\omega_c\right)}{\omega_c\left(n_ds^2+n_ps+n_i\right)}\end{vmatrix}=0. \tag{30}$$

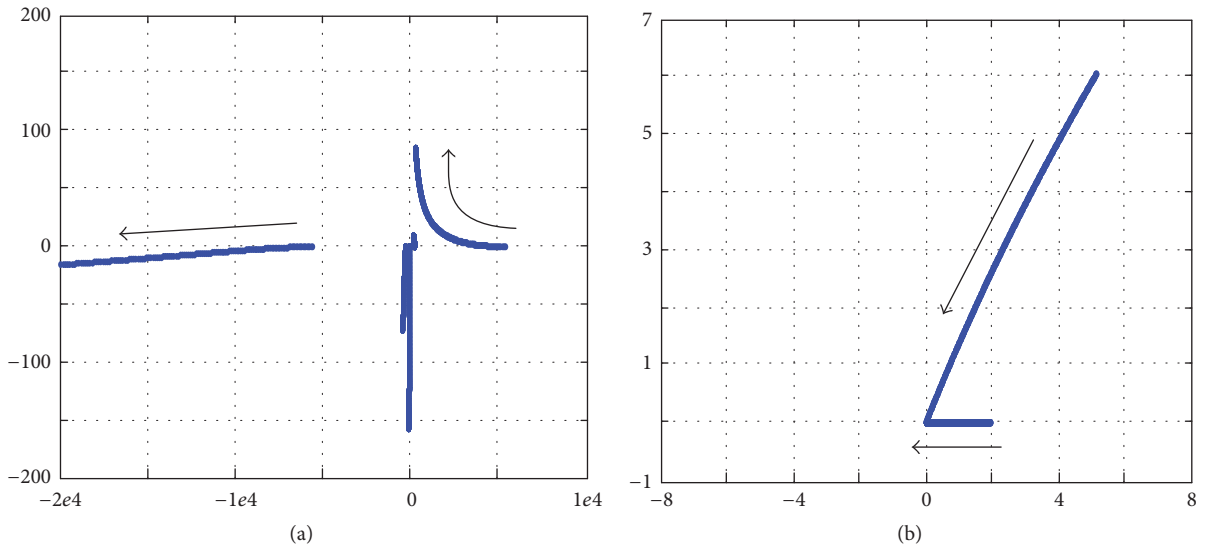

Figure 6: The root locus of the small-signal model based on the traditional power calculation method.

Table 1: Parameters table.

R/Ω	0.1
R_o/Ω	48.4
E_{1e}/V	220
E_{2e}/V	220
φ_{1e}	$-1e-3$
φ_{2e}	$-1e-3$
ω_c/rad/s	62.8

The model established by (30) is a six-order system, and its physical meaning is aimed at the whole parallel system while the traditional small-signal model established by (9) is aimed at the single inverter only. Although the model established by (30) is simpler than the model by Marwali et al., it still cannot be analyzed directly and is required to be solved by mathematical tools such as MATLAB.

5. Analysis of the New Small-Signal Model

5.1. Small-Signal Model of Traditional Power Calculation Method. First, the model established by the traditional power calculation method is analyzed, the circuit parameters are given in Table 1, and it is should be noted that the steady-state values should be satisfied (21). Figure 6 is a root locus of the small-signal model using the traditional power calculation method. (a) is the local root locus when n_i is equal to 1 and m_p increases from 0 to 1, and (b) is the local root locus when m_p is equal to 1 and n_i decreases from $1e-2$ to $1e-5$. Observing Figure 6, we discover that the parallel system, using traditional power calculation method, is not stable in the root locus, for which the traditional power calculation method will introduce an AC variable of double frequency. In order to suppress the oscillation, m_p should be increased or n_i should be decreased.

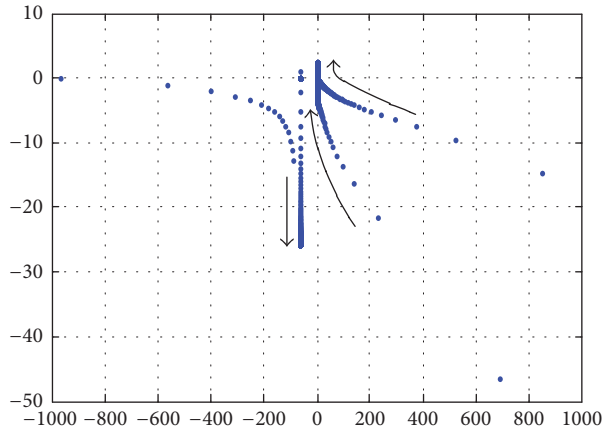

Figure 7: The root locus of the small-signal model based on the traditional power calculation method.

Figure 7 is a root locus of the small-signal model based on the traditional power calculation method after introducing differential control. The droop coefficients are as follows: $n_i = 1e-3$, $m_p = 1e-1$, $n_p = 1e-4$, and $m_d = 1e-4$, and n_d increases from 0 to $8e-3$. We can discover from the Table 1 that, after introducing differential control, a pair of conjugate complex roots are generated. This is the basic reason why the dynamic response of the model can be improved.

5.2. Small-Signal Model of the New Power Calculation Method. From the small-signal model, established by the traditional power calculation method, it can be found that the robustness of the parallel inverter is not strong. In order to improve it, the author uses the new power calculation method without a large delay low-pass filter, and this paper regards the model based on the new power calculation method as the main analysis object.

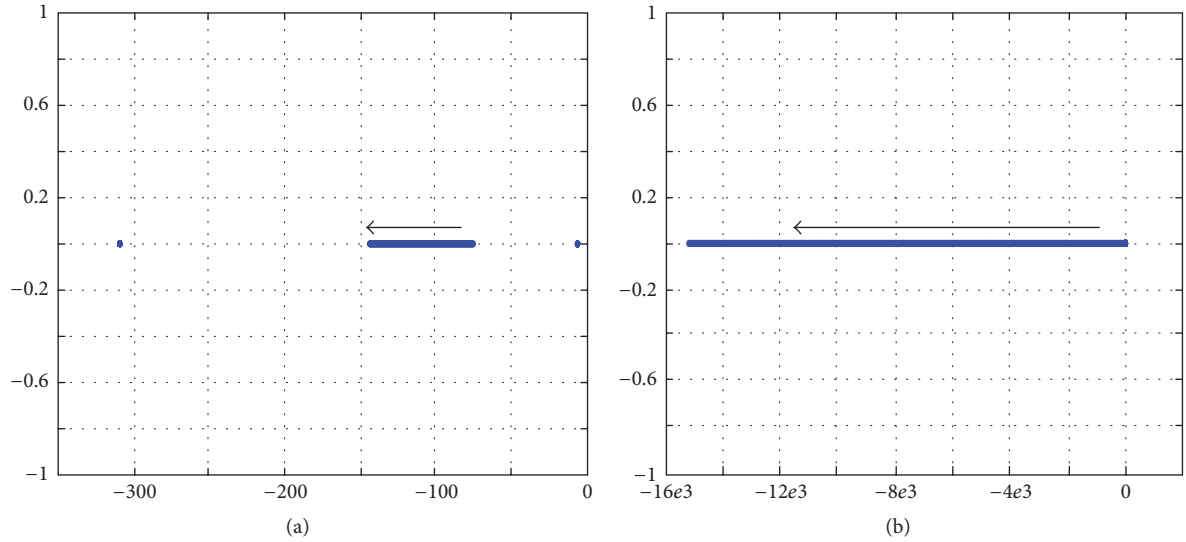

Figure 8: The root locus of a small-signal model based on the new power calculation method.

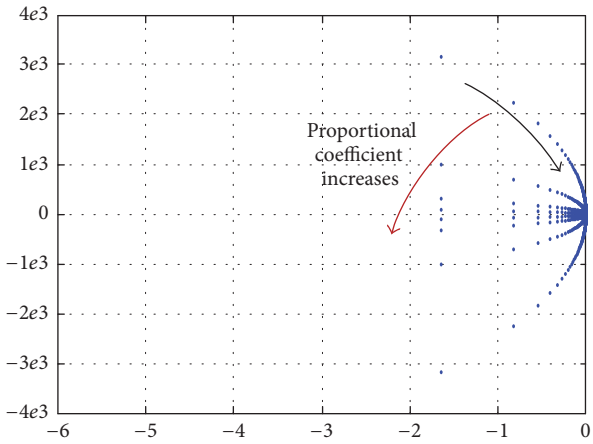

Figure 9: The root locus after a differential controller is used.

Figure 8 is the root locus of the small-signal model based on the new power calculation method only using proportional droop control. (a) is the root locus when n_i is equal to $1e-4$ and m_p increases from 0 to $1e-2$, and (b) is the root locus when m_p is equal to $1e-4$ and n_i increases from 0 to $5e-3$. Three important points can be obtained from Figure 8: firstly, the new power calculation method is better than the traditional power calculation method, and the poles always fall on the left side of the imaginary axis; secondly, when only the proportional droop is adopted, the poles fall on the negative real axis, which indicates that the dynamic performance is good; thirdly, with the increase of the proportional droop coefficient, the poles of the system shift to the left and the stability is improved.

Figure 9 is the root locus of the small-signal model based on the new power calculation method with differential control. In Figure 9, $n_p = m_d = 0$, and the four curves correspond to four local root locus, respectively, when $n_i = m_p = 1e-1$, $1e-2$, $1e-3$, and $1e-4$ and n_d increases from 0 to $1e-5$. From Figure 9, we can discover that the introduction of differential control generates conjugate complex roots. And the significance of the conjugate complex roots is to improve the dynamic performance of the system, but the excessive increase of the differential coefficient will lead to the instability of the system. In addition, it can be found in Figure 9 that the increase of the proportional droop coefficient will lead the poles to move to the left and increase the stability of the system.

The control parameters of Figure 10(a) are as follows: $m_p = 1e-2$, $n_i = 1e-2$, $n_d = 5e-7$, and $m_d = 0$, and n_p increases from 0 to $1e-4$. The control parameters of Figure 10(b) are as follows: $m_p = 1e{-}2, n_i = 1e{-}2, n_d = 5e{-}7$, and $n_p = 5e{-}5$, and m_d increases from 0 to $1e{-}4$. Figure 10(a) indicates that n_p mainly affects the conjugate complex roots and can be modified to fine-tune the dynamic response of the system. m_d mainly affects the poles on the negative real axis, but this pole is not the main pole. So its influence on the system performance is not very large.

Figure 11 is the root locus when the impedance varies, and all the droop coefficients are given as follows: $m_p = 1e-2$, $n_i = 1e{-}2, n_d = 5e{-}7, n_p = 5e{-}5$, and $m_d = 1e{-}8$. (a) is the root locus when R_o increases from $1e-2$ to $1e2$ and (b) is the root locus when R_o increases from $1e{-}3$ to $5e{-}1$. (a) indicates that with the increase of resistance, that is, the load decrease, the poles on the negative real roots move to two sides of the axis, respectively, but the main poles are getting closer to the imaginary axis. So the stability of the system becomes worse when the load becomes smaller. (b) shows that, with a change of the output impedance of the inverter, the pole moves to the right but the main pole has not been changed. So a change of the output impedance has a limited effect on the parallel system.

Figure 12 is the root locus when the cut-off frequency of the low-pass filter increases from $1e-2$ to 20, and the droop coefficients used are the same as those in Figure 11. Figure 12 shows that, to a certain extent, the system gets more stable if

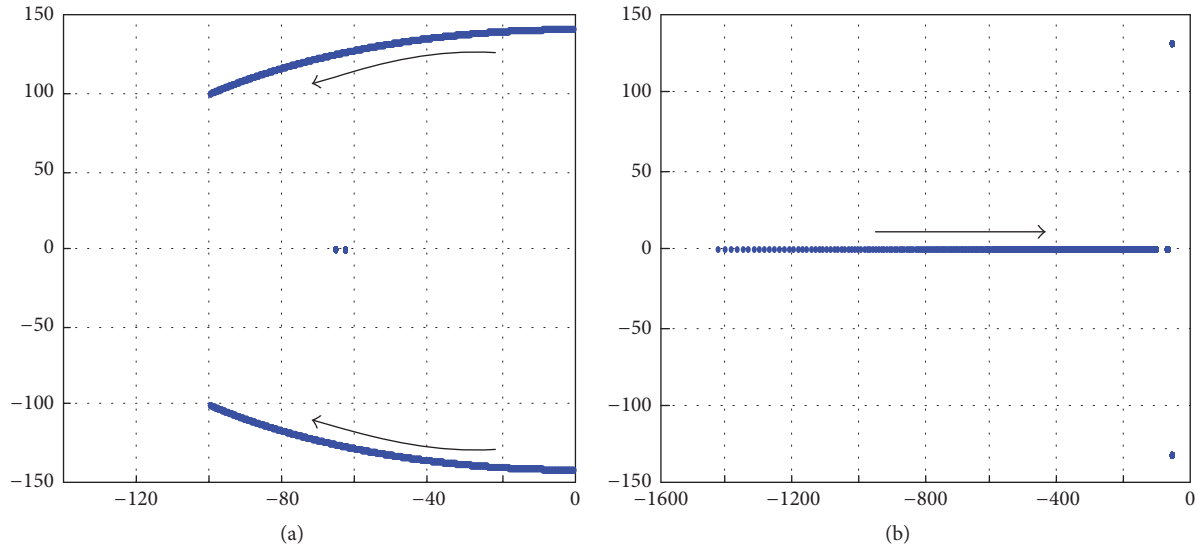

Figure 10: The root locus of the small-signal model based on the traditional power calculation method.

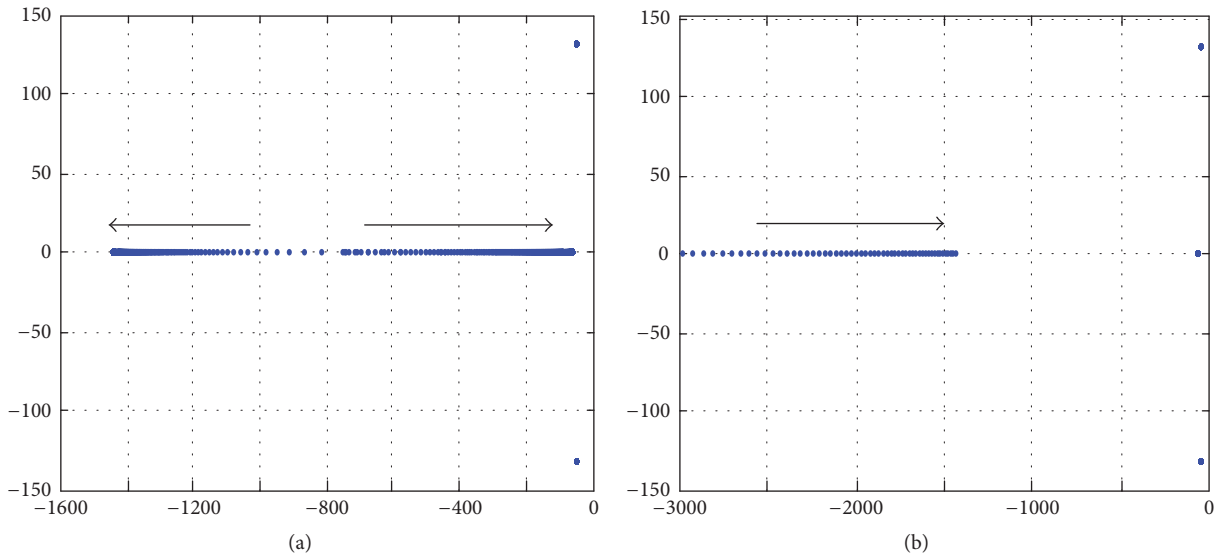

Figure 11: The root locus when impedance varies.

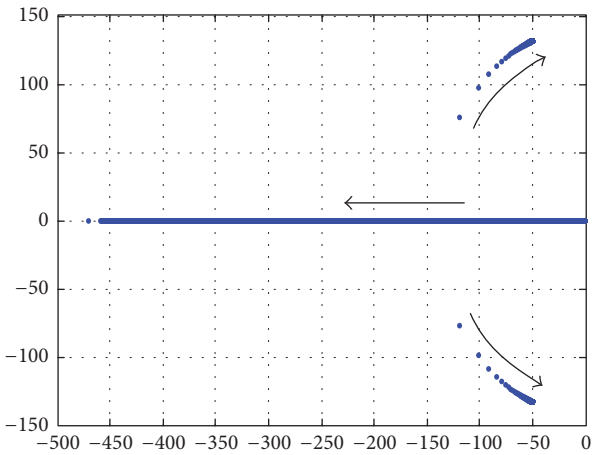

Figure 12: The root locus when ω_c varies.

the cut-off frequency is increased, but the cut-off frequency cannot increase without limit. When the cut-off frequency increases to a certain value, the main pole of the system turns into a pair of conjugate complex roots that move right with the increase of the cut-off frequency. Then the system stability will get worse.

6. The Research on Application of the Model

Based on the small-signal model introduced in the this paper and the droop control that we researched before, the problem of unbalanced current and harmonic current caused by the unbalanced and nonlinear loads can be resolved and the output current can be shared equally. Thus, this part establishes the simulated and experimented platform to verify the theory. The simulated and experimental parameters are

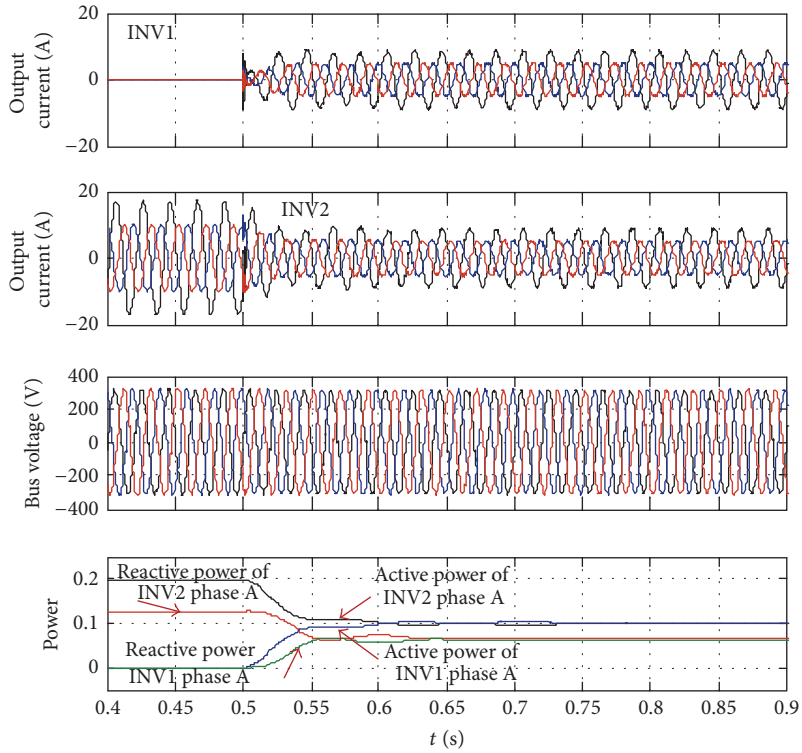

Figure 13: The simulated results with an unbalanced load.

Table 2: Parameters of simulation and experiment.

Sampling time T_s/s	$1e-4$
Switching frequency/Hz	5k
Filter inductance L/mH	1.5
Parasitic inductance r/mΩ	270
Filter capacitor C/μF	20
Midline inductance L_n/mH	2
Rated voltage/V	220

all within the range of previous stability analysis so that the correctness of the stability analysis can be well verified.

The simulated model is built by using Simulink/s-function. Power is expressed by per unit value and 1 means 11375 kVA. The simulated parameters are shown in Table 2.

First, the simulated results and analysis of the control strategy in the parallel inverter system with an unbalanced load are introduced as follows. Figure 13 is the unbalanced load simulated results waveform, which indicates that the unbalanced currents can be shared effectively.

Second, the simulated results and analysis of the control strategy in the parallel inverter system with a nonlinear load are illustrated, and Figure 14 is the nonlinear load simulated waveforms, which indicates that the proposed droop method can share harmonic currents effectively.

The experimental results and analysis of the parallel inverter system with an unbalanced load are described as follows. Figure 15 is the experimental unbalanced load waveforms, and we can discover that the unbalanced current can

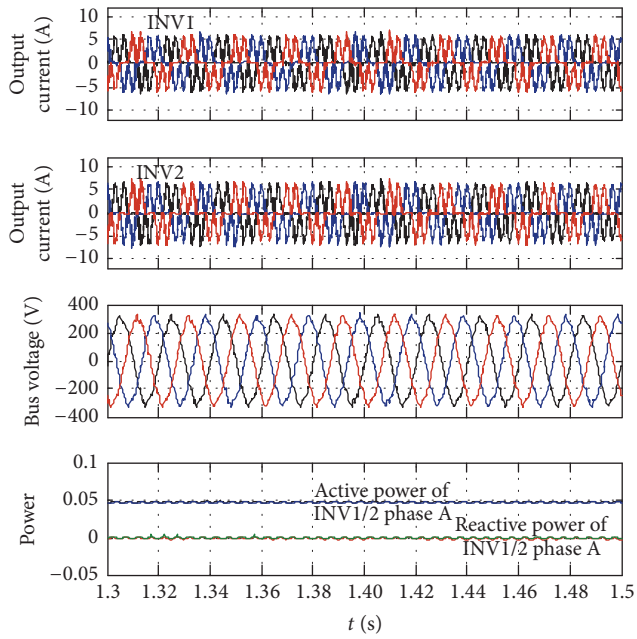

Figure 14: The simulated results with a nonlinear load.

be accurately shared. The experimental results are consistent with the simulated results.

Similarly, the experimental results and analysis of the nonlinear load are introduced. Figure 16 is the experimental waveforms with a nonlinear load, which indicates that the

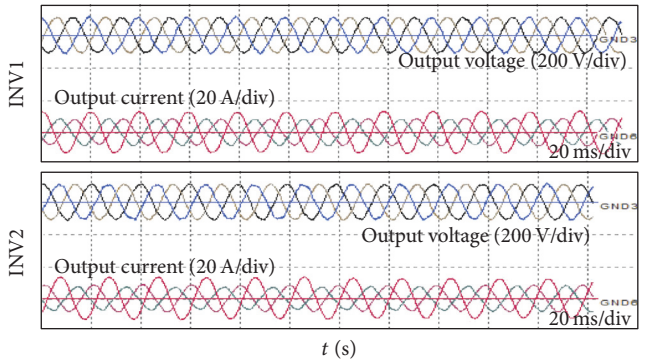

Figure 15: The experimental results with an unbalanced load.

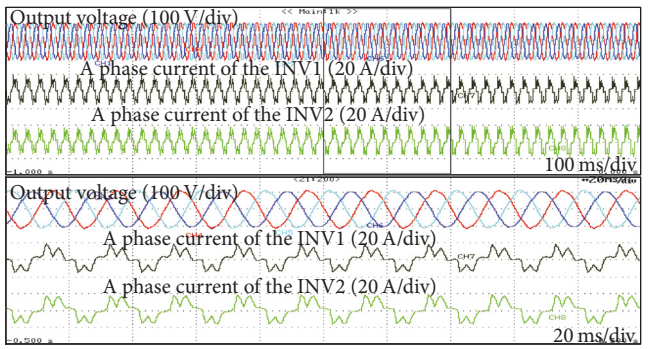

Figure 16: The experimental results with a nonlinear load.

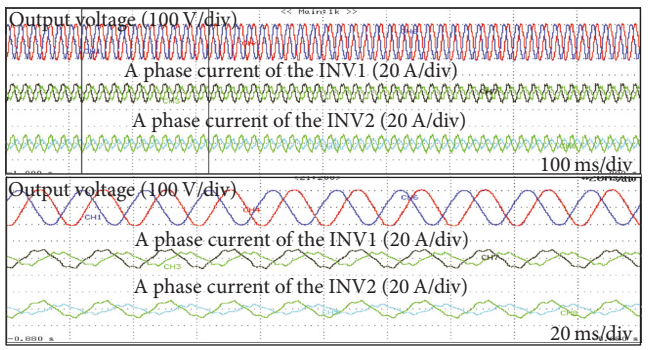

Figure 17: The experimental results with an unbalanced and nonlinear load.

proposed droop method can share harmonic currents accurately and has good robustness.

Figure 17 is the experimental waveforms with an unbalanced load and nonlinear load at the same time. It can be seen from the figure that the unbalanced and harmonic currents can both be effectively shared.

Figure 18 is a photograph of the experimental platform. All the experiments in this paper were completed using this experimental platform.

7. Conclusions

This paper proposes a new small-signal modeling method for an auxiliary parallel inverter system and analyzes the influence of the parameters on the stability characteristics of the system in detail. The traditional analysis method is based on a small-signal model, but the model established by the traditional small-signal method is not accurate without considering the coupling relationship between parallel inverters, so this model cannot analyze the influence of the load and the output impedance of inverter. The small-signal modeling method proposed in this paper regards the whole parallel system as the research object, including the influences of the control system information outside the voltage loop and circuit parameters of inverter, which provide the most comprehensive analysis method by far.

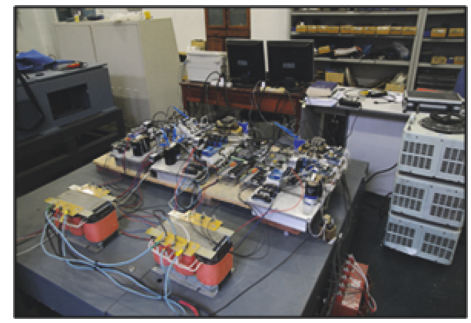

Figure 18: The photograph of experiment platform.

Appendix

A. The Coefficient Matrix D of Traditional Method

The coefficient matrix D of the traditional power calculation method is as follows:

$$d_{11} = \frac{dp_1}{d\varphi_1} = \frac{-2R_o\left(R+R_o\right)E_1^2\sin 2\varphi_1 - R_oRE_1E_2\sin\left(\varphi_1+\varphi_2\right)}{R\left(R+2R_o\right)^2} + j \cdot \frac{2R_o\left(R+R_o\right)E_1^2\cos 2\varphi_1 + R_oRE_1E_2\cos\left(\varphi_1+\varphi_2\right)}{R\left(R+2R_o\right)^2},$$

$$d_{21} = \frac{dq_1}{d\varphi_1} = \frac{2R_o\left(R+R_o\right)E_1^2\cos 2\varphi_1 + R_oRE_1E_2\cos\left(\varphi_1+\varphi_2\right)}{R\left(R+2R_o\right)^2} + j\frac{2R_o\left(R+R_o\right)E_1^2\sin 2\varphi_1 + R_oRE_1E_2\sin\left(\varphi_1+\varphi_2\right)}{R\left(R+2R_o\right)^2},$$

$$d_{31} = \frac{dp_2}{d\varphi_1} = \frac{-R_oRE_1E_2\sin\left(\varphi_1+\varphi_2\right) + 2R_o^2E_1^2\sin 2\varphi_1}{R\left(R+2R_o\right)^2} + j\frac{R_oRE_1E_2\cos\left(\varphi_1+\varphi_2\right) - 2R_o^2E_1^2\cos 2\varphi_1}{R\left(R+2R_o\right)^2},$$

$$d_{41} = \frac{dq_2}{d\varphi_1} = \frac{R_o R E_1 E_2 \cos(\varphi_1 + \varphi_2) - 2R_o^2 E_1^2 \cos 2\varphi_1}{R(R + 2R_o)^2} + j\frac{R_o R E_1 E_2 \sin(\varphi_1 + \varphi_2) - 2R_o^2 E_1^2 \sin 2\varphi_1}{R(R + 2R_o)^2},$$

$$d_{12} = \frac{dp_1}{d\varphi_2} = \frac{2R_o^2 E_2^2 \sin 2\varphi_2 - R_o R E_1 E_2 \sin(\varphi_1 + \varphi_2)}{R(R + 2R_o)^2} + j\frac{-2R_o^2 E_2^2 \cos 2\varphi_2 + R_o R E_1 E_2 \cos(\varphi_1 + \varphi_2)}{R(R + 2R_o)^2},$$

$$d_{22} = \frac{dq_1}{d\varphi_2} = \frac{-2R_o^2 E_2^2 \cos 2\varphi_2 + R_o R E_1 E_2 \cos(\varphi_1 + \varphi_2)}{R(R + 2R_o)^2} - j\frac{2R_o^2 E_2^2 \sin 2\varphi_2 - R_o R E_1 E_2 \sin(\varphi_1 + \varphi_2)}{R(R + 2R_o)^2},$$

$$d_{32} = \frac{dp_2}{d\varphi_2} = \frac{-R_o R E_1 E_2 \sin(\varphi_1 + \varphi_2) - 2R_o(R + R_o) E_2^2 \sin 2\varphi_2}{R(R + 2R_o)^2} + j \cdot \frac{R_o R E_1 E_2 \cos(\varphi_1 + \varphi_2) + 2R_o(R + R_o) E_2^2 \cos 2\varphi_2}{R(R + 2R_o)^2},$$

$$d_{42} = \frac{dq_2}{d\varphi_2} = \frac{R_o R E_1 E_2 \cos(\varphi_1 + \varphi_2) + 2R_o(R + R_o) E_2^2 \cos 2\varphi_2}{R(R + 2R_o)^2} + j\frac{R_o R E_1 E_2 \sin(\varphi_1 + \varphi_2) + 2R_o(R + R_o) E_2^2 \sin 2\varphi_2}{R(R + 2R_o)^2},$$

$$d_{13} = \frac{dp_1}{dE_1} = \frac{2R_o(R + R_o) E_1 \cos 2\varphi_1 + R_o R E_2 \cos(\varphi_1 + \varphi_2)}{R(R + 2R_o)^2} + j\frac{2R_o(R + R_o) E_1 \sin 2\varphi_1 + R_o R E_2 \sin(\varphi_1 + \varphi_2)}{R(R + 2R_o)^2},$$

$$d_{23} = \frac{dq_1}{dE_1} = \frac{2R_o(R + R_o) E_1 \sin 2\varphi_1 + R_o R E_2 \sin(\varphi_1 + \varphi_2)}{R(R + 2R_o)^2} - j \cdot \frac{2R_o(R + R_o) E_1 \cos 2\varphi_1 + R_o R E_2 \cos(\varphi_1 + \varphi_2)}{R(R + 2R_o)^2},$$

$$d_{33} = \frac{dp_2}{dE_1} = \frac{R_o R E_2 \cos(\varphi_1 + \varphi_2) - 2R_o^2 E_1 \cos 2\varphi_1}{R(R + 2R_o)^2} + j \cdot \frac{R_o R E_2 \sin(\varphi_1 + \varphi_2) - 2R_o^2 E_1 \sin 2\varphi_1}{R(R + 2R_o)^2},$$

$$d_{43} = \frac{dq_2}{dE_1} = \frac{R_o R E_2 \sin(\varphi_1 + \varphi_2) - 2R_o^2 E_1 \sin 2\varphi_1}{R(R + 2R_o)^2} - j \cdot \frac{R_o R E_2 \cos(\varphi_1 + \varphi_2) - 2R_o^2 E_1 \cos 2\varphi_1}{R(R + 2R_o)^2},$$

$$d_{14} = \frac{dp_1}{dE_2} = \frac{-2R_o^2 E_2 \cos 2\varphi_2 + R_o R E_1 \cos(\varphi_1 + \varphi_2)}{R(R + 2R_o)^2} + j\frac{-2R_o^2 E_2 \sin 2\varphi_2 + R_o R E_1 \sin(\varphi_1 + \varphi_2)}{R(R + 2R_o)^2},$$

$$d_{24} = \frac{dq_1}{dE_2} = \frac{-2R_o^2 E_2 \sin 2\varphi_2 + R_o R E_1 \sin(\varphi_1 + \varphi_2)}{R(R + 2R_o)^2} - j \cdot \frac{-2R_o^2 E_2 \cos 2\varphi_2 + R_o R E_1 \cos(\varphi_1 + \varphi_2)}{R(R + 2R_o)^2},$$

$$d_{34} = \frac{dp_2}{dE_2} = \frac{R_o R E_1 \cos(\varphi_1 + \varphi_2) + 2R_o(R + R_o) E_2 \cos 2\varphi_2}{R(R + 2R_o)^2} + j\frac{R_o R E_1 \sin(\varphi_1 + \varphi_2) + 2R_o(R + R_o) E_2 \sin 2\varphi_2}{R(R + 2R_o)^2},$$

$$d_{44} = \frac{dq_2}{dE_2} = \frac{R_o R E_1 \sin(\varphi_1 + \varphi_2) + 2R_o(R + R_o) E_2 \sin 2\varphi_2}{R(R + 2R_o)^2} - j \cdot \frac{R_o R E_1 \cos(\varphi_1 + \varphi_2) + 2R_o(R + R_o) E_2 \cos 2\varphi_2}{R(R + 2R_o)^2}. \quad \text{(A.1)}$$

B. The Coefficient Matrix D of New Method

The coefficient matrix D of the new power calculation method is as follows:

$$d_{11} = \frac{dp_1}{d\varphi_1} = \frac{-R_o R E_1 E_2 \sin(\varphi_1 - \varphi_2)}{R(R + 2R_o)^2},$$

$$d_{21} = \frac{dq_1}{d\varphi_1} = \frac{-\left(R_o R + 2R_o^2\right) E_1 E_2 \cos(\varphi_1 - \varphi_2)}{R(R + 2R_o)^2},$$

$$d_{31} = \frac{dp_2}{d\varphi_1} = \frac{-R_o R E_1 E_2 \sin(\varphi_1 - \varphi_2)}{R(R + 2R_o)^2},$$

$$d_{41} = \frac{dq_2}{d\varphi_1} = \frac{\left(R_o R + 2R_o^2\right) E_1 E_2 \cos(\varphi_1 - \varphi_2)}{R(R + 2R_o)^2},$$

$$
\begin{aligned}
d_{12} &= \frac{dp_1}{d\varphi_2} = \frac{R_o R E_1 E_2 \sin(\varphi_1 - \varphi_2)}{R(R+2R_o)^2},\\
d_{22} &= \frac{dq_1}{d\varphi_2} = \frac{(R_o R + 2R_o^2) E_1 E_2 \cos(\varphi_1 - \varphi_2)}{R(R+2R_o)^2},\\
d_{32} &= \frac{dp_2}{d\varphi_2} = \frac{R_o R E_1 E_2 \sin(\varphi_1 - \varphi_2)}{R(R+2R_o)^2},\\
d_{42} &= \frac{dq_2}{d\varphi_2} = \frac{-(R_o R + 2R_o^2) E_1 E_2 \cos(\varphi_1 - \varphi_2)}{R(R+2R_o)^2},\\
d_{13} &= \frac{dp_1}{dE_1}\\
&= \frac{2R_o(R+R_o)E_1 + R_o R E_2 \cos(\varphi_1 - \varphi_2)}{R(R+2R_o)^2},\\
d_{23} &= \frac{dq_1}{dE_1} = \frac{-(R_o R + 2R_o^2) E_2 \sin(\varphi_1 - \varphi_2)}{R(R+2R_o)^2},\\
d_{33} &= \frac{dp_2}{dE_1} = \frac{R_o R E_2 \cos(\varphi_1 - \varphi_2) - 2R_o^2 E_1}{R(R+2R_o)^2},\\
d_{43} &= \frac{dq_2}{dE_1} = \frac{(R_o R + 2R_o^2) E_2 \sin(\varphi_1 - \varphi_2)}{R(R+2R_o)^2},\\
d_{14} &= \frac{dp_1}{dE_2} = \frac{-2R_o^2 E_2 + R_o R E_1 \cos(\varphi_1 - \varphi_2)}{R(R+2R_o)^2},\\
d_{24} &= \frac{dq_1}{dE_2} = \frac{-(R_o R + 2R_o^2) E_1 \sin(\varphi_1 - \varphi_2)}{R(R+2R_o)^2},\\
d_{34} &= \frac{dp_2}{dE_2}\\
&= \frac{R_o R E_1 \cos(\varphi_1 - \varphi_2) + 2R_o(R+R_o)E_2}{R(R+2R_o)^2},\\
d_{44} &= \frac{dq_2}{dE_2} = \frac{(R_o R + 2R_o^2) E_1 \sin(\varphi_1 - \varphi_2)}{R(R+2R_o)^2}.
\end{aligned}
\tag{B.1}
$$

C. The Coefficients of Traditional Method

The coefficients of traditional power calculation method are given as follows:

$$
\begin{aligned}
a_1 &= R_o(R+R_o)E_1^2 \cos 2\varphi_1 - R_o^2 E_2^2 \cos 2\varphi_2\\
&\quad + R_o R E_1 E_2 \cos(\varphi_1 + \varphi_2),\\
b_1 &= R_o(R+R_o)E_1^2 \sin 2\varphi_1 - R_o^2 E_2^2 \sin 2\varphi_2\\
&\quad + R_o R E_1 E_2 \sin(\varphi_1 + \varphi_2),\\
c_1 &= R_o(R+R_o)E_1^2 \sin 2\varphi_1 - R_o^2 E_2^2 \sin 2\varphi_2\\
&\quad + R_o R E_1 E_2 \sin(\varphi_1 + \varphi_2),\\
d_1 &= -R_o(R+R_o)E_1^2 \cos 2\varphi_1 + R_o^2 E_2^2 \cos 2\varphi_2\\
&\quad - R_o R E_1 E_2 \cos(\varphi_1 + \varphi_2),\\
a_2 &= R_o R E_1 E_2 \cos(\varphi_1 + \varphi_2)\\
&\quad + R_o(R+R_o)E_2^2 \cos 2\varphi_2 - R_o^2 E_1^2 \cos 2\varphi_1,\\
b_2 &= R_o R E_1 E_2 \sin(\varphi_1 + \varphi_2)\\
&\quad + R_o(R+R_o)E_2^2 \sin 2\varphi_2 - R_o^2 E_1^2 \sin 2\varphi_1,\\
c_2 &= R_o R E_1 E_2 \sin(\varphi_1 + \varphi_2)\\
&\quad + R_o(R+R_o)E_2^2 \sin 2\varphi_2 - R_o^2 E_1^2 \sin 2\varphi_1,\\
d_2 &= -R_o R E_1 E_2 \cos(\varphi_1 + \varphi_2)\\
&\quad - R_o(R+R_o)E_2^2 \cos 2\varphi_2 + R_o^2 E_1^2 \cos 2\varphi_1.
\end{aligned}
\tag{C.1}
$$

D. The Coefficients of New Method

The coefficients of new power calculation method are given as follows:

$$
\begin{aligned}
&\widetilde{p}_1\\
&= \frac{R_o(R+R_o)E_1^2 - R_o^2 E_2^2 + R_o R E_1 E_2 \cos(\varphi_1 - \varphi_2)}{R(R+2R_o)^2},\\
&\widetilde{q}_1 = \frac{-(R_o R + 2R_o^2) E_1 E_2 \sin(\varphi_1 - \varphi_2)}{R(R+2R_o)^2},\\
&\widetilde{p}_2\\
&= \frac{R_o R E_1 E_2 \cos(\varphi_1 - \varphi_2) + R_o(R+R_o)E_2^2 - R_o^2 E_1^2}{R(R+2R_o)^2},\\
&\widetilde{q}_2 = \frac{(R_o R + 2R_o^2) E_1 E_2 \sin(\varphi_1 - \varphi_2)}{R(R+2R_o)^2}.
\end{aligned}
\tag{D.1}
$$

Conflicts of Interest

The authors declare that there are no conflicts of interest regarding the publication of this paper.

Acknowledgments

This work was supported by the Basic Scientific Research Project of Central University (Grant no. 2016RC038) and National Key R&D Plan (Grant no. 2016YFB1200502).

References

[1] Q. Shafiee, J. M. Guerrero, and J. C. Vasquez, "Distributed secondary control for islanded microgrids-a novel approach," *IEEE Transactions on Power Electronics*, vol. 29, no. 2, pp. 1018–1031, 2014.

[2] H. Jiefeng, Z. Jianguo, D. G. Dorrell, and J. M. Guerrero, "Virtual flux droop method - a new control strategy of inverters in microgrids," *IEEE Transactions on Power Electronics*, vol. 29, no. 9, pp. 4704–4711, 2014.

[3] W. Yao, M. Chen, J. Matas, J. M. Guerrero, and Z.-M. Qian, "Design and analysis of the droop control method for parallel inverters considering the impact of the complex impedance on the power sharing," *IEEE Transactions on Industrial Electronics*, vol. 58, no. 2, pp. 576–588, 2011.

[4] Y. Shi, W. Wu, H. Wang, Y. Du, and J. Su, "The Parallel Multi-Inverter System Based on the Voltage-Type Droop Control Method," *IEEE Journal of Emerging and Selected Topics in Power Electronics*, vol. 4, no. 4, pp. 1332–1341, 2016.

[5] J. M. Guerrero, J. C. Vasquez, J. Matas, L. G. de Vicuña, and M. Castilla, "Hierarchical control of droop-controlled AC and DC microgrids: a general approach toward standardization," *IEEE Transactions on Industrial Electronics*, vol. 58, no. 1, pp. 158–172, 2011.

[6] Y. Wei, C. Min, J. Matas, J. M. Guerrero, and Z.-M. Qian, "Design and analysis of the droop control method for parallel inverters considering the impact of the complex impedance on the power sharing," *IEEE Transactions on Industrial Electronics*, vol. 58, no. 2, pp. 576–588, 2011.

[7] J. Chen, L. Wang, L. Diao, H. Du, and Z. Liu, "Distributed auxiliary inverter of urban rail train-load sharing control strategy under complicated operation condition," *IEEE Transactions on Power Electronics*, vol. 31, no. 3, pp. 2518–2529, 2016.

[8] H. Ming, H. Haibing, Y. Xing, and J. M. Guerrero, "Multilayer control for inverters in parallel operation without intercommunications," *IEEE Transactions on Power Electronics*, vol. 27, no. 8, pp. 3651–3663, 2012.

[9] Y. Wei, M. Chen, J. Matas, J. M. Guerrero, and Z.-M. Qian, "Design and analysis of the droop control method for parallel inverters considering the impact of the complex impedance on the power sharing," *IEEE Transactions on Industrial Electronics*, vol. 58, no. 2, pp. 576–588, 2011.

[10] J. M. Guerrero, J. C. Vasquez, J. Matas, M. Castilla, and L. G. de Vicuña, "Control strategy for flexible microgrid based on parallel line-interactive UPS systems," *IEEE Transactions on Industrial Electronics*, vol. 56, no. 3, pp. 726–736, 2009.

[11] T. Wu, Z. Liu, J. Liu, S. Wang, and Z. You, "A Unified Virtual Power Decoupling Method for Droop-Controlled Parallel Inverters in Microgrids," *IEEE Transactions on Power Electronics*, vol. 31, no. 8, pp. 5587–5603, 2016.

[12] J. C. Vasquez, J. M. Guerrero, M. Savaghebi, J. Eloy-Garcia, and R. Teodorescu, "Modeling, analysis, and design of stationary-reference-frame droop-controlled parallel three-phase voltage source inverters," *IEEE Transactions on Industrial Electronics*, vol. 60, no. 4, pp. 1271–1280, 2013.

[13] E. Antonio, A. Coelho, P. C. Cortizo, P. Francisco, and D. Garcia, "Small signal stability for single phase inverter connected to stiff AC system," in *Proceedings of the 1999 IEEE Industry Applications Conference - 34th IAS Annual Meeting*, pp. 2180–2187, October 1999.

[14] Y. Cheng, X. Zha, and H. Chen, "The small signal model for wireless parallel operation of inverters," in *Proceedings of the 2009 IEEE International Conference on Mechatronics and Automation, ICMA 2009*, pp. 433–437, chn, August 2009.

[15] F. Gao, Z. Li, Y. Li, P. Wang, and H. Zhu, "Small-signal stability analysis of parallel-connected inverters based on time-varying phasor," in *Proceedings of the 2011 6th IEEE Conference on Industrial Electronics and Applications, ICIEA 2011*, pp. 1239–1244, chn, June 2011.

[16] E. A. A. Coelho, P. C. Cortizo, and P. F. D. Garcia, "Small-signal stability for parallel-connected inverters in stand-alone ac supply systems," *IEEE Transactions on Industry Applications*, vol. 38, no. 2, pp. 533–542, 2002.

[17] M. N. Marwali, J.-W. Jung, and A. Keyhani, "Stability analysis of load sharing control for distributed generation systems," *IEEE Transactions on Energy Conversion*, vol. 22, no. 3, pp. 737–745, 2007.

[18] M. Hua, H. Hu, Y. Xing, and J. M. Guerrero, "Multilayer control for inverters in parallel operation without intercommunications," *IEEE Transactions on Power Electronics*, vol. 27, no. 8, pp. 3651–3663, 2012.

[19] S. J. Chiang and J. M. Chang, "Parallel control of the UPS inverters with frequency-dependent droop scheme," in *Proceedings of the 2001 IEEE 32nd Annual Power Electronics Specialists Conference*, pp. 957–961, can, June 2001.

[20] B. Ning, T. Tang, H. Dong et al., "An introduction to parallel control and management for high-speed railway systems," *IEEE Transactions on Intelligent Transportation Systems*, vol. 12, no. 4, pp. 1473–1483, 2011.

[21] S. Xu, J. Wang, and J. Xu, "A current decoupling parallel control strategy of single-phase inverter with voltage and current dual closed-loop feedback," *IEEE Transactions on Industrial Electronics*, vol. 60, no. 4, pp. 1306–1313, 2013.

[22] X. Wei, K. Dai, X. Fang, P. Geng, F. Luo, and Y. Kang, "Parallel Control of Three-Phase Three-Wire Shunt Active Power Filters," in *Proceedings of the 2006 CES/IEEE 5th International Power Electronics and Motion Control Conference*, pp. 1–5, Shanghai, China, August 2006.

[23] Q.-J. Kong, L. Li, B. Yan, S. Lin, F. Zhu, and G. Xiong, "Developing parallel control and management for urban traffic systems," *IEEE Intelligent Systems*, vol. 28, no. 3, pp. 66–69, 2013.

[24] J. M. Guerrero, L. G. de Vicuña, J. Matas, M. Castilla, and J. Miret, "A wireless controller to enhance dynamic performance of parallel inverters in distributed generation systems," *IEEE Transactions on Power Electronics*, vol. 19, no. 5, pp. 1205–1213, 2004.

[25] X. Wei, G. Zhu, J. Lu, and X. Xu, "Instantaneous current-sharing control scheme of multi-inverter modules in parallel based on virtual circulating impedance," *IET Power Electronics*, vol. 9, no. 5, pp. 960–968, 2016.

[26] Q. Lei, F. Z. Peng, and S. Yang, "Multiloop control method for high-performance microgrid inverter through load voltage and current decoupling with only output voltage feedback," *IEEE Transactions on Power Electronics*, vol. 26, no. 3, pp. 953–960, 2011.

[27] H. Ming, H. Hu, Y. Xing, and J. M. Guerrero, "Multilayer control for inverters in parallel operation without intercommunications," *IEEE Transactions on Power Electronics*, vol. 27, no. 8, pp. 3651–3663, 2012.

[28] S. Golestan, M. Monfared, J. M. Guerrero, and M. Joorabian, "A D-Q synchronous frame controller for single-phase inverters," in *Proceedings of the 2011 2nd Power Electronics, Drive Systems and Technologies Conference, PEDSTC 2011*, pp. 317–323, irn, February 2011.

[29] Z. Ren, M. Gao, Q. Mo et al., "Power calculation method used in wireless parallel inverters under nonlinear load conditions," in *Proceedings of the 25th Annual IEEE Applied Power Electronics Conference and Exposition, APEC 2010*, pp. 1674–1677, usa, February 2010.

[30] D. Sutanto, H. R. Outhred, and Y. B. Lee, "Probabilistic power system production cost and reliability calculation by the z-transform method," *IEEE Transactions on Energy Conversion*, vol. 4, no. 4, pp. 559–566, 1989.